Molecular dynamics methodology to investigate steady-state heterogeneous crystal growth

J. Vatamanu and P. G. Kusalik[a)]
Department of Chemistry, University of Calgary, 2500 University Drive NW, Calgary, Alberta T2N1N4, Canada

(Received 11 September 2006; accepted 23 January 2007; published online 23 March 2007)

In this paper a new molecular dynamics simulation methodology to investigate steady-state heterogeneous crystal growth from a supercooled liquid is presented. The method is tested on pure component systems such as Lennard-Jonesium and water/ice, as well as multicomponent systems such as methane hydrate crystals. The setup uses periodicity in all three directions and two interfaces; at one interface, crystallization occurs, while at the other, melting is enforced by locally heating the crystal only near that interface. Steady-state conditions are achieved when the crystal is melted at the same rate as the growth occurs. A self-adaptive scheme that automatically modifies the rate of melting to match the rate of growth, crucial for establishing steady-state conditions, is described. In contrast with the recently developed method of Razul *et al.* [Mol. Phys. **103**, 1929 (2005)], where the rates of growth (melting) were constant and the temperatures determined, the present approach fixes the supercooling temperature at the growing interface and identifies the corresponding steady-state crystal growth rate that corresponds to the thermodynamic force provided. The static properties of the interface (e.g., the interfacial widths) and the kinetics of the crystal growth are found to reproduce well previous findings. The importance of establishing steady-state conditions in such investigations is also briefly discussed. © *2007 American Institute of Physics*. [DOI: 10.1063/1.2710263]

I. INTRODUCTION

Heterogeneous crystal growth is of tremendous important from both practical and theoretical points of view.[1] The latter viewpoint focuses on fundamental questions regarding the underlying processes involved in molecular ordering of a liquid at a crystalline interface.[2] It is well recognized today that atomistic simulations of interfacial phenomena and heterogeneous growth can provide an alternate and reliable approach to experiment.[3] For example, simulation predictions for interfacial widths, complex patterns, and diffusion processes on interfaces are to a significant degree consistent with experimental data.[3,4]

Although crystallization has been reasonably extensively investigated by means of atomistic simulations, there are only a few methodologies that actually achieve steady-state heterogeneous crystal growth.[5–10] Many previous studies have used a simulation system with slab geometry, where nonperiodicity is assigned in the direction of crystal growth. However, in such approaches, two more interfaces, vacuum (or wall)/crystal and vacuum/liquid, are implicitly or explicitly introduced. The liquid/solid interface of interest can be affected by the presence of these additional interfaces, particularly if placed closer than 25 Å to it. Moreover, during growth in slab geometry, the composition of the system will change, and thus it is impossible to attain a steady state in such a setup. We remark that performing heterogeneous crystal growth under steady-state conditions can be critically important when the properties of the interface are of interest; only under steady-state conditions will the interface and its properties be time invariant and therefore can be appropriately statistically sampled. Additional complications and computational overhead in slab geometry may also arise from the special two-dimensional Ewald methods required to handle long-range interactions in such geometries.

The early work of Broughton *et al.*[6] provided a means through which to study apparent steady-state crystal growth in atomic systems. In their approach the authors employed periodicity in essentially only two directions, where atomic layers were effectively streamed through the system.[6] A recently developed approach reported by Razul *et al.*[8] has been successfully employed to achieve steady-state crystal growth of both atomic and molecular liquids, as pure and mixed systems.[8–11] In this approach, the temperature was controlled by two local thermostats, one hot and one cold. In the presence of the imposed temperature gradient, one interface was above the melting temperature and exhibited melting, while at the second interface crystallization occurred due to its undercooling. Steady-state crystal growth was driven by moving the thermostats (and hence the temperature gradient) through the simulation box. Except for the two areas where the local thermostats were applied, the dynamics within the system was Newtonian ensuring that the processes at the interfaces arise only from the interactions between molecules and not from the fictitious forces of the thermostats.

These previous studies[8–10] indicate that heterogeneous crystal growth is inherently a stochastic process, and therefore the underlying details of the microscopic dynamics are not important; what is critical is that the fluctuations that lead

[a)]Electronic mail: peter.kusalik@ucalgary.ca

to ordering/disordering be appropriately sampled. Thus, macroscopic rates of growth, average interface properties, and the nature of the molecular configurations that lead to ordering can be shown[11] not to depend in any significant way on the specific ensemble utilized in the simulation.

Despite its utility, there are several disadvantages inherent in the temperature gradient methodology. To drive the crystal growth and to constrain reasonably the interfaces to the moving frame of the temperature gradient, values that are rather large on a macroscopic scale (10^6–10^7 K/cm) are required. The presence of the temperature gradient has the undesirable effect of distorting somewhat the profile functions of various properties measured across the interface. This can be problematic, particularly in the pressure where it leads to development of local stresses in the solid region. For success in multicomponent systems, the correct velocity of the thermostats, the right composition in solution, and the right temperature at the interface need to be triangulated within a relatively small domain. This can make achievement of steady-state growth in some systems rather challenging with this approach.

In order to avoid many of the above mentioned difficulties, we have developed, implemented, and successfully tested a setup that uses a constant (undercooled) temperature across the whole system except for a small region at the melting interface, where a temperature pulse provides the required high temperature conditions. To achieve steady states, the rate of movement of the temperature pulse must equal the rate of crystal growth. Therefore, in this setup, the system will crystallize at the rate appropriate for the degree of undercooling provided. However, the interface is free to fluctuate unconstrained by the presence of a temperature gradient. As will be discussed below, the challenge in this approach is the maintenance of steady-state conditions, particularly for one-component systems. To this end, a self-adaptive scheme for the establishment and maintenance of steady-state crystal growth is demonstrated. The scope of this paper is to provide and test a useful framework for investigation of steady-state crystal growth for a broad class of systems. This method has now been successfully applied to simulations of heterogeneous crystal growth for a variety of systems (see Ref. 12).

This paper is organized as follows. In the next section we describe our molecular dynamics (MD) methodology to investigate heterogeneous crystal growth. In Sec. III we test this approach, and results are presented for the crystal growth on various crystal faces of Lennard-Jonesium (LJ) systems, hexagonal ice, and methane hydrates. A summary of our findings, advantages and shortcomings of this approach, as well as implications to crystal growth studies, will then be discussed in Sec. IV.

II. METHODOLOGY

A schematic of the present methodology is presented in Fig. 1. The system consists of two solid/liquid interfaces separating liquid and crystal phases. The majority of the system and the interface where crystallization occurs are at a temperature slightly below the thermodynamic melting temperature of the crystal. At the second interface, where the crystal is melting, a temperature pulse is applied. In general, to achieve steady-state heterogeneous crystal growth and hence constant compositional parameters, the velocity of the heat pulse, the rate of crystal growth, and the rate of melting must be equal. Perhaps the most straightforward scheme to achieve a temperature profile as required in our setup consists of a Nose-Hoover (NH) chain[13] thermostat on each molecule with the target temperature as a function of the molecule's position normal to interface (along the z direction). The equations of motion of the thermostat variables are described by the following generic set of relationships:[13]

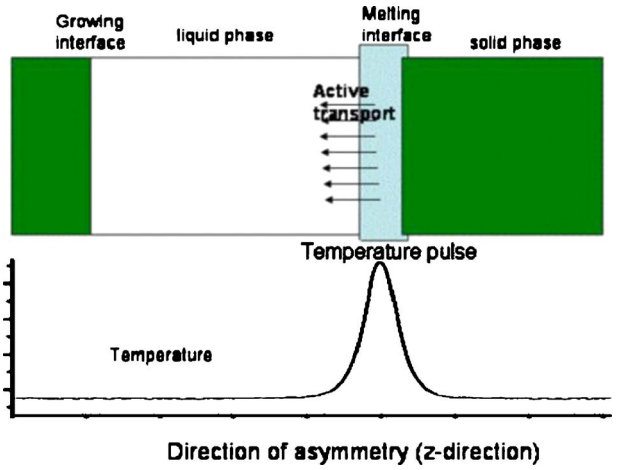

FIG. 1. (Color online) Schematic representation of the simulation cell together with the profile of the temperature through the system. The temperature in the system is constant except for a small region around the melting interface where a Gaussian-shaped temperature pulse is applied. The use of two interfaces allows for periodicity in all three directions and steady-state crystal growth to be attained.

$$\begin{aligned}
\frac{d\xi_i^{(1)}}{dt} &= \left(\frac{T_i^{\mathrm{calc}}}{T^{\mathrm{imp}}(z)} - 1\right)\frac{1}{Q^{(1)}} - \xi_i^{(1)}\xi_i^{(2)}, \\
\frac{d\xi_i^{(2)}}{dt} &= \left(\frac{(\xi_i^{(1)})^2}{Q^{(1)}} - 1\right)\frac{1}{Q^{(2)}} - \xi_i^{(2)}\xi_i^{(3)}, \\
\frac{d\xi_i^{(3)}}{dt} &= \left(\frac{(\xi_i^{(2)})^2}{Q^{(2)}} - 1\right)\frac{1}{Q^{(3)}} - \xi_i^{(3)}\xi_i^{(4)}, \\
\frac{d\xi_i^{(4)}}{dt} &= \left(\frac{(\xi_i^{(3)})^2}{Q^{(3)}} - 1\right)\frac{1}{Q^{(4)}},
\end{aligned} \tag{1}$$

where the size of the NH chains is 4 and the subscript i is the molecular index. $\xi_i^{(1)}$, $\xi_i^{(2)}$, $\xi_i^{(3)}$, and $\xi_i^{(4)}$ are the NH thermostat variables for chains (1), (2), (3) and (4), respectively, while the Q^k are the inertia masses of the thermostat chains. The above relationships adjust the thermostat variables such that the instantaneous (rotational or translational) temperatures T_i^{calc} of each molecule i are adjusted toward the imposed (bath) temperature $T^{\mathrm{imp}}(z)$ that now depends on its z position in the simulation box.

The translational equations of motion for the molecular linear momentum p_i can be expressed as

$$dp_i/dt = F_i + \xi^{(1)}_{i,\text{translate}} p_i - \gamma_i, \tag{2}$$

where F_i is the total force acting on molecule i due to its interactions with all other molecules in the system and the $\xi^{(1)}_{i,\text{translate}}$ arises from the thermostat on the molecule i. In addition to the usual terms due to force fields and thermostats, Eq. (2) contains an extra term γ_i that is required to ensure the conservation of the total linear momentum of the system. The conservation of linear momentum must be strictly (analytically) imposed; otherwise artifacts due to nonzero net momentum could contaminate the melting/crystallizing processes at the interfaces. Since the sum of the individual particle forces must be zero, it follows that to conserve the total linear momentum the relationship

$$\sum_i \gamma_i = -\sum_i (\xi^{(1)}_{i,\text{translate}} p_i) \tag{3}$$

must be satisfied. There is no unique way to assign a specific value to γ_i for each molecule in Eq. (3). Perhaps the most straightforward approach to satisfy this constraint is to distribute it uniformly over all molecules so that

$$\gamma_i = -\frac{1}{N}\sum_j (\xi^{(1)}_{j,\text{translate}} p_j), \tag{4}$$

where N is the total number of molecules in the system. A more general scheme could incorporate a desired weighting factor w_i, such that

$$\gamma_i = -w_i \sum_j (\xi^{(1)}_{j,\text{translate}} p_j), \qquad \sum_i w_i = 1. \tag{5}$$

The use of the weighting scheme given by Eq. (5) could be beneficial if the molecular dynamics needs to be changed from its standard form only locally (e.g., preferentially near the temperature pulse).

For the rotational degrees of freedom, no special care is needed to conserve the angular momentum (it is already not conserved in periodic boundary conditions). The relationship for the rotational motion therefore retains its standard form and can be found in any standard reference.[14]

The above scheme can be used to grow crystals from mixtures or solutions. However, we note that an additional complication may arise in the case of mixtures because of the large differences in the time scales of the processes involved. For example, in the case of methane hydrate crystals, this scheme requires the mass transport of methane from the melting to the growing interface. To help address this issue, we have typically applied a small external fictitious force to methane molecules that effectively shuttles the methane along the z direction over a small distance from the melting towards the growing interface. We have called this technique "active transport."[10] This force is given by

$$F^{\text{active}}_{B,j}(z) = E_0 w_j(z), \tag{6}$$

where B labels the component species activated (e.g., methane in our case), E_0 is roughly 1%–2% of the average force that a molecule, j, of component B experiences in the liquid environment, and $w_j(z)$ is a weighting function that localizes the active transport intensity to a certain region of the system. For $w(z)$ we typically use a truncated and zoomed Gaussian centered at a certain position in the box,

$$w(z) = \frac{\exp(-((z-z_0)/\gamma)^2) - \exp(-(c/\gamma)^2)}{1 - \exp(-(c/\gamma)^2)}, \tag{7}$$

where γ is the width of the Gaussian and c is the cutoff distance beyond which the active transport has been turned off. In our runs the maximum of $w(z)$ was centered at the position of the temperature pulse, c was set at 10 Å, and γ was set to 16 Å. The use of active transport has the side affect of generating a bulk linear momentum. To conserve linear momentum, the total net force generated by Eq. (6) must be balanced by additional forces redistributed over "nonactivated" molecular species (e.g., other than B), such that only a few molecules located within less important regions in the system have their dynamics modified (see Ref. 10 for details).

When using a temperature pulse or active transport, it would be preferable to alter the equation of motions from their standard form only over a limited region well away from the interfaces of interest. At the growing interface the sampling can therefore be canonical (or *NPT* if desired). Although the dynamics at the interfaces is not Newtonian as in our previous work,[8–10] such a setup has the advantage that it allows one to sample from other desired ensembles and the growing interface is no longer subject to a temperature gradient.

In the present approach, the system can find its own rate of growth at a specified temperature. This present challenges if steady-state growth conditions are desired. Even if the (average) rate of growth is known in advance with very good accuracy, heterogeneous crystal growth will not be sustainable over long times in a finite sample at a constant growth rate. This is because the inherent fluctuations in the interface (due to the stochastic nature of the underlying ordering and disordering processes) will asymptotically cause a finite system to diverge from a steady state. For a one-component system, we have found that the system will always completely melt or crystallize given a sufficiently long simulation run, no matter how carefully the (constant) growth rate was chosen.

Since it is very desirable to control heterogeneous crystal growth, we have developed a self-adaptive procedure that monitors the growth rate on the fly and maintains the system at a given steady state. In our procedure, the growth rates are adjusted regularly (after a fixed number of MD time steps) according to the feedback mechanism that satisfies an imposed restriction in the system. For feedback, we have used in the case of pure systems a constant predefined distance between the two interfaces or between the growing interface and the position of the temperature pulse (typically set to be about half of the simulation box length). The rate of movement of the temperature pulse was then modified using a simple Berdensen-like scheme,

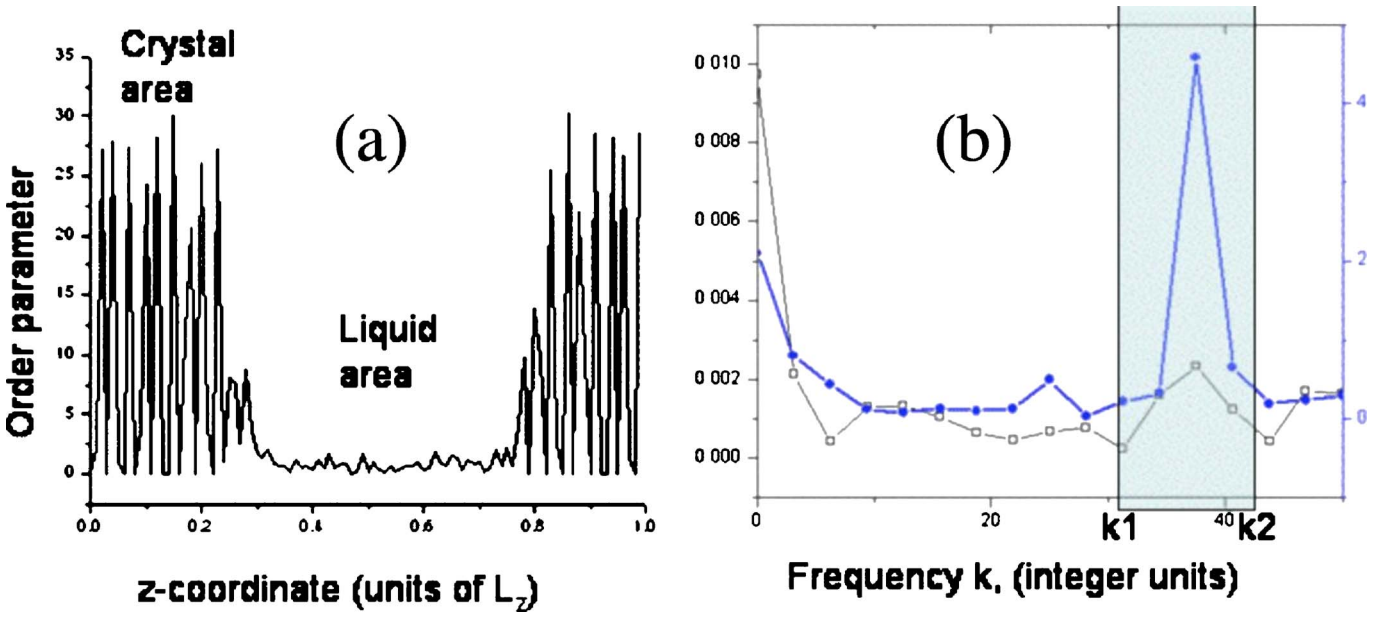

FIG. 2. (Color online) (a) $\chi(z)$ order parameter and (b) its Fourier spectrum for crystalline (blue line) and liquid (black line) parts of the system. Clearly the crystalline part generates a peak in its Fourier spectrum that is absent in the liquid.

$$r_t = r_{t-1} + \frac{1}{C}(\Delta z - \Delta z_0), \tag{8}$$

where r_{t-1} is the rate of moving the temperature pulse from the previous step, Δz_0 and Δz are the imposed and measured distances between the two interfaces, respectively, and C is an adjustable coupling constant (with units of time). When the system grows faster than it melts, the distance between the two interfaces (across the liquid) Δz becomes smaller, and if it is less than the imposed distance Δz_0, then the scheme given by Eq. (8) will increase the velocity of the temperature pulse.

In the case of mixtures, a desired rate can be determined by monitoring the composition. For example, for methane hydrates, one may adjust the melting rate such that a certain methane composition is maintained in the liquid. Thus the velocity of the temperature pulse becomes

$$r_t = r_{t-1} + \frac{1}{C}([CH_4] - [CH_4]_0), \tag{9}$$

where $[CH_4]$ and $[CH_4]_0$ are the imposed and the measured concentrations of methane in the solution, respectively.

In order to implement the scheme given by Eq. (8), a criterion that discriminates between crystal and liquid phases is required. Such a criterion must be generic yet powerful enough to identify relatively accurately the position of the interface using data from only a small number of time steps (i.e., less than 1000). One such criterion is based on the fact that the crystal phase has certain (positional) symmetry detectable as a signature in a Fourier spectrum that is expected to be absent in liquids. We have tested the profiles of both densities and structural order parameters from instantaneous and time-averaged configurations as candidates to locate the position of the interface. As an example, in Fig. 2, the $\chi(z)$ profile of a typical LJ liquid/solid system is presented. Clearly, in the solid phase, there are oscillations in this structural order parameter [see Eqs. (7) of Ref. 8] that have a specific frequency in Fourier space, while for the liquid, the intensity of this signal is essentially zero.

As a discriminating criterion, we can use the quantity

$$d(z) = A^{(\mathrm{left})}(z) - A^{(\mathrm{right})}(z), \tag{10}$$

where $A^{(\mathrm{left})}(z)$ is the area under a specific peak of the Fourier spectrum, $P^{(\mathrm{left})}(z,k)$, of the order parameter's z profile computed from the position z in the system towards the left part of the box, while $A^{(\mathrm{right})}(z)$ is the area of the same peak in the power spectrum, $P^{(\mathrm{right})}(z,k)$, obtained from the right part of the box.

Our procedure to evaluate $A^{(\mathrm{left})}(z)$ and $A^{(\mathrm{right})}(z)$ is as follows. (1) Evaluate the order parameter $\chi(z)$ (or density profile) on a grid of $N^{(z)}$ points along the z direction over a short period of time (from 1 to 100 time steps). (2) At any z-grid point, select a specific number of points $n^{(z)}$ towards the left side (decreasing z) and build the vector $\chi_l^{(\mathrm{left})}(z)$, $l=1,\ldots,n^{(z)}$. In similar fashion, build the vector $\chi_l^{(\mathrm{right})}(z)$, $l=1,\ldots,n^{(z)}$ with $n^{(z)}$ points taken towards the right part (increasing z) of the box. We note that the periodicity of the system must be explicitly taken into account when building the vectors $\chi_l^{(\mathrm{left})}(z)$ and $\chi_l^{(\mathrm{right})}(z)$ and that there must be $N^{(z)}$ such vectors. (3) Evaluate the Fourier transforms $P^{(\mathrm{left})}(z,k)$ and $P^{(\mathrm{right})}(z,k)$ of the vectors $\chi_l^{(\mathrm{left})}(z)$ and $\chi_l^{(\mathrm{right})}(z)$, respectively, where k is the Fourier space coordinate. (4) $A^{(\mathrm{left})}(z)$ and $A^{(\mathrm{right})}(z)$ are obtained by integrating $P^{(\mathrm{left})}(z,k)$ and $P^{(\mathrm{right})}(z,k)$, respectively, over the specific range of k corresponding to the identified peak for the crystal. In our runs, the evaluation of the z profiles for the density or $\chi(z)$ was done on a grid of $N^{(z)}=128$ points, while $A^{(\mathrm{left})}(z)$ and $A^{(\mathrm{right})}(z)$ were evaluated using $\chi_l^{(\mathrm{left})}(z)$ and $\chi_l^{(\mathrm{right})}(z)$ vectors of size $n^{(z)}=32$ or 64 points. With this scheme we were able to determine the current position of the interfaces with a precision of 0.4–0.5 molecular diameters.

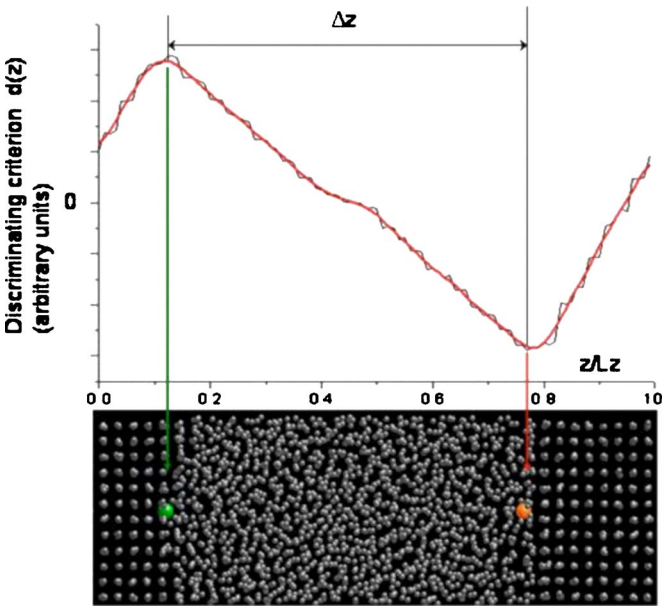

FIG. 3. (Color online) The discriminating criterion based on differences of Fourier spectrum area as measured from a given position z toward the left part and the right part of the box. The maximum and minimum indicated by the green and blue lines represent the positions of growing and melting interfaces, respectively. The black line represents the raw data, while the red line is a three-point FFT smoothing of the raw data. The configurational snapshot shown to scale below the graph helps visualize how well the discrimination criterion identifies the positions of the interfaces (see also the red and blue spheres that have been highlighted within the interfaces). The quantity Δz is the measured instantaneous distance between the two interfaces.

At the crystallizing interface in the present setup, the value of $A^{(\mathrm{left})}(z)$ will mostly reflect crystal (a large peak in the Fourier spectrum), while $A^{(\mathrm{right})}(z)$ will result from mostly liquid; therefore at this point a maximum in the magnitude of the discriminating criterion will be observed. The typical shape of $d(z)$ is presented in Fig. 3. Interestingly, there is no need to know an absolute value of $d(z)$ to obtain the location of the interface, and only the positions of its extrema are required.

III. RESULTS AND DISCUSSIONS

In this section we present the application and the performance of the present approach in the steady-state heterogeneous crystal growth of the following: LJ systems, hexagonal ice I, and sI methane hydrates. The ability of the methodology to establish and maintain stable steady states, the quality of predicted kinetics of the growth, as well as the interfacial widths and z profiles of several properties of interest will be analyzed.

A. Simulations details

Results will be presented here for the growth of the [001], [011], and [111] faces of a LJ crystal, of three different faces of hexagonal ice, and sI methane hydrate. The [001] LJ systems contained 2592, 5888, and 13 248 particles corresponding to box sizes of $8\sigma\times8\sigma\times40\sigma$, $13\sigma\times13\sigma\times40\sigma$, and $19\sigma\times19\sigma\times40\sigma$, respectively. The [011] LJ systems had 544, 1632, 6528, and 16 320 atoms within box sizes of $4.7\sigma\times3.3\sigma\times40\sigma$, $7\sigma\times6.6\sigma\times40\sigma$, $13.7\sigma\times12.9\sigma\times41.6\sigma$, and $22.8\sigma\times19.4\sigma\times41.6\sigma$, respectively. In the case of the [111] LJ systems, box sizes of the $4.7\sigma\times4\sigma\times37.3\sigma$, $9.2\sigma\times8\sigma\times40.8\sigma$, $13.7\sigma\times11.8\sigma\times37.2\sigma$ and $22.8\sigma\times23.7\sigma\times37.2\sigma$ containing 624, 2496, 5616, and 18 720 molecules, respectively, were employed. It was found that LJ systems with fewer than 1000 atoms exhibited strong system size effects and were too small to be considered for further analysis. For hexagonal ice (I) we utilized systems of 2688 molecules (with a cross section of 27.13×31.33 Å^2) for the [0001] face, 2496 molecules (cross section of 27.1×29.5 Å^2) for the [1010] face, and 2816 molecules (29.45×31.23 Å^2) for the [1−210] face. The runs with ice were performed at two different temperatures, 265 and 255 K, utilizing the six-site water model of Nada and van der Eerden.[15] In the case of methane hydrate, a [001] face system consisting of $2\times2\times12$ unit cells[16] of methane hydrate was considered. By removing about 35% of the initial methane, a two-phase system consisting of a methane hydrate crystal and a supersaturated methane aqueous solution was prepared as a starting point for further production runs. We have modeled the water with the TIP4P potential[17] and methane by a single LJ site.[18] The short-range forces were evaluated with a cutoff of 3.35σ for LJ systems with more than 5000 molecules, and otherwise 0.06σ less than half of the simulation box width. For water/ice and methane hydrate systems, a cutoff of 11.2 Å was employed. The electrostatic forces were evaluated with the fast smooth particle mesh Ewald method[19] using interpolating splines of sixth order and a Fourier grid of roughly 1 point/Å. The equations of motions were integrated with a fourth order predictor-corrector algorithm. Nose-Hoover chain thermostats were employed on each molecules as described in Sec. II. In this study, an anisotropic Berdensen barostat was employed for constant pressure runs.

A typical MD run required the following steps:

(1) *NPT* thermalization of the crystal adjusts the temperature and pressure of the system to their desired values.
(2) In the preparation of the two-phase system, we have applied a short high temperature pulse to a small region for a short time to initiate the melting of the crystal in that area. Then, using a step temperature profile (with temperature regions above and below the melting temperature), a two-phase system was prepared, with about 50% liquid and 50% crystal. The final (desired) temperature profile was established and a barostat was applied to readjust the pressure as required.
(3) During heterogeneous growth itself, the temperature pulse was moved through the system such that the amount of crystal melted equals the amount of crystal formed at the second interface (i.e., a steady state is maintained). In our *NVT* production runs, this step was started as *NPT* (to allow for better control of the pressure), and then after steady state was reached the barostat was turned off.

B. Discrimination between solidlike and liquidlike molecules

In our analysis and in the figures presented below, we have labeled the molecules based on their solidlike and liquidlike characters. The criterion employed to establish solid- or liquidlike character utilizes single molecule properties, and it is important to note that this criterion is different from the fast Fourier transform (FFT) based method presented in Sec. II that pinpoints the position of the interface.

The method we have employed to distinguish between liquidlike and solidlike molecules is based on a measure that accounts for the local diffusive translational and rotational motion.[8] Specifically, for a trajectory segment of length N steps, we recorded the displacement

$$\delta_i = \sum_{t=1}^{N \text{ steps}} (R_{i,t} - \langle R_i \rangle)^2, \tag{11}$$

where $R_{i,t}$ is the instantaneous position of molecule i at time step t, while the $\langle R_i \rangle$ is the average position of molecule i over that particular trajectory segment. If the motion of the molecule is limited (as in the crystal phase), then the value of δ_i will be small, less than a predetermined threshold, and the molecule will be labeled as solidlike. Otherwise, when a molecule's mean square displacement (msd) about its mean position excesses the threshold, it is labeled as liquidlike. Typically, solidlike or liquidlike character was determined from a molecule's history over roughly 10–100 ps. To exemplify how this dynamic criterion works in the current systems, we present in Fig. 4 for a typical LJ system a three-dimensional (3D) plot of δ_i versus trajectory segment length and position in the box along the z direction. As expected, δ_i increases with trajectory segment length in the liquid phase while remaining almost constant in the solid region of the box [see Fig. 4(a)]. To help better visualize how this msd criterion captures the position of the interfaces, a surface plot of δ_i from Fig. 4(a) is shown alongside a configurational snapshot in Fig. 4(b). It is clearly evident from Fig. 4 that this criterion compares very well to the corresponding structural snapshot and thus captures well the position of the interface. We have found that the position and widths estimated from msd profiles agree very well with those obtained from other measures.

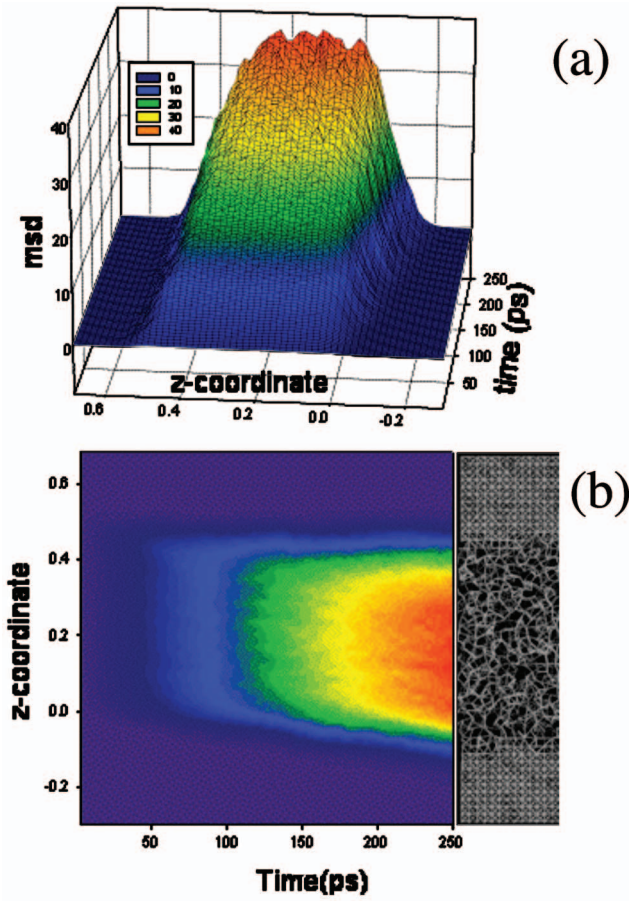

FIG. 4. (Color) (a) 3D plot of translational msd from an average position vs simulation trajectory segment length and position in the box. (b) A surface plot of the data in (a) with a configurational snapshot given on the right to illustrate how well this dynamic criterion captures the positions of the interfaces. The z coordinate is in units of length of the simulation box in the z direction and is measured relative to the position of the temperature pulse. This plot for the translational msd is typical for all the systems investigated here and indicates that it can be used as a new type of profile function to characterize the position and widths of the interfaces.

C. LJ systems

We have tested the proposed methodology on three crystallographic faces of a LJ system, [001], [011], and [111], and at several levels of undercooling. In these simulations we have found that the estimated instantaneous rate of growth is neither constant nor of particular interest here since it is dominated by the fluctuations of the system. Rather we focus on the net kinetics of the process as characterized by the average rate of growth. An obvious question regarding the stability of such an approach is how much the instantaneous rates can fluctuate about an average rate such that the system does not diverge from its steady state. The answer to this question will obviously depend on the coupling constant C in Eq. (8). Therefore it is important to determine what "reasonable" values of C are. From extensive investigations of many LJ systems at different temperatures (and hence rates of growth) and with various system sizes, we classify the coupling constant C as strong when $C/\Delta t$ is about 10^8 (where Δt is the time step), while values of 10^{10}–10^{11} are considered to represent weak coupling. In Fig. 5, a plot of instantaneous and average rates is presented for a [001] LJ system for strong coupling of the motion of the temperature pulse. In this run only the positive values of r [see Eq. (8)] were allowed, and hence the moving frame only followed fluctuations consistent with crystal growth. The averaged rates of growth were evaluated as the running averages of the instantaneous rates. In spite of the large changes observed in the instantaneous rates, the average rate was a well converged quantity after 800 000 time steps, and the system did not diverge from its steady state. This result indicates that the proposed self-adaptive method of growth can be quite robust.

The time dependence of the instantaneous rates presented in Fig. 5 indicates that the system effectively pushes the temperature pulse forward from time to time as crystallization occurs. It is important to point out that there is no

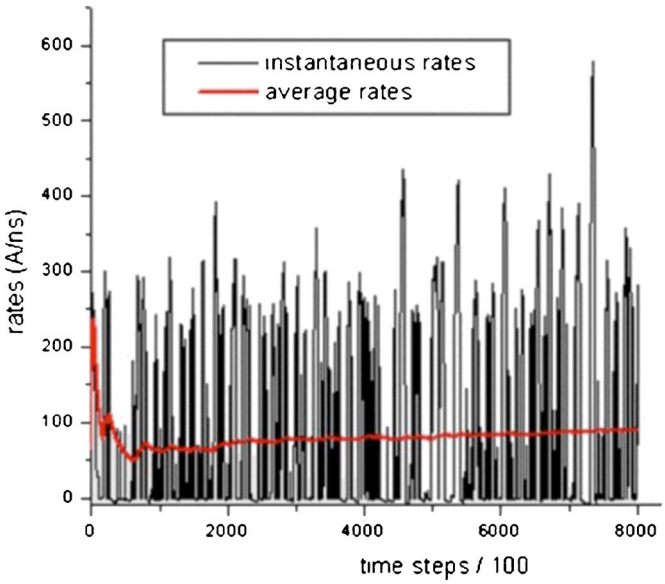

FIG. 5. (Color online) Instantaneous and running average rates of growth for a LJ system on the [001] face at a temperature of 0.608 (in reduced units). The average growing rate is converged after 200 000 time steps even when large changes in the motion of the temperature pulse were allowed.

intrinsic periodicity in the apparent behavior of the instantaneous growth rates; rather they simply reflect the fluctuations of the growing interface. To confirm this we have performed growth simulations with different coupling constants. We have found that the time dependence of the instantaneous rates varies with the coupling constant in a manner that indicates a response dominated by the effective inertia of the temperature pulse [see Eq. (8)]. For larger coupling constants, the changes in instantaneous rates were smaller than those presented in Fig. 5, while the average rates were independent of this value, as expected.

In order to reach steady-state growth by the means of a self-adaptive scheme, it is critically important to find a quantity that identifies the position of the growing interface with reasonable accuracy in as few as one time step. The results presented below use the differences in Fourier spectra of the instantaneous density. To help quantify how precise such a criterion can be, statistics for the predicted position of the interface is presented in Table I for three LJ systems at a reduced temperature of 0.608 and a coupling constant of $10^9\Delta t$, a value about ten times smaller than the coupling used

TABLE I. The evaluation of the interfacial positions during steady-state crystal growth of the [001], [011], and [111] crystallographic faces of a LJ system. Column 2 gives the average position of the growing interface relative to the temperature pulse. Columns 3 and 4 indicate the extreme deviations toward the solid and liquid phases, respectively, from the average position of interface. The values are in units of the z-dimensional box length, where the simulation box was between 100 and 140 Å along its z direction. The results are from runs of 800 000 time steps.

Crystallographic face	Average position	Min.	Max.	Standard deviation
001	0.510	0.46	0.59	0.018
011	0.507	0.44	0.59	0.019
111	0.560	0.35	0.74	0.069

TABLE II. The average rates of heterogeneous crystal growth for the [001] and [011] crystallographic faces of a LJ system as a function of temperature. The temperatures are given in Kelvin and the rates in Å/ns as for argon LJ parameters, while the numbers in parentheses are the corresponding values in reduced units.

Temperature	[001]	[011]
78 (0.650)	−140 (−0.088)	−164 (−0.10)
75 (0.625)	18 (0.011)	9 (0.005)
74 (0.616)	64 (0.040)	29 (0.018)
73 (0.608)	90 (0.057)	72 (0.045)
72 (0.600)	138 (0.087)	87 (0.055)
70 (0.583)	192 (0.121)	147 (0.093)
67 (0.558)	291 (0.184)	195 (0.123)

in most of our production runs. Obviously, for smaller coupling constants, the deviations from the average value of the predicted position of the interface will be smaller. Both the [001] and [011] faces have small standard deviations of the position, while the [111] face has a larger value. This arises due to the fact that the parametrization of the self-adaptive algorithm was optimized for growth on the [001] face. Although this implementation was successful in achieving steady-state growth on the [111] face, a further refinement of the parameters in the algorithm should be possible.

The average rates of growth obtained for the [001] and [011] faces of a LJ crystal are given in Table II. We note that the negative rates indicate that the system is melting. While these results were obtained in the *NPT* ensemble, switching to the *NVT* ensemble results in no significant changes in the growth rates. This further emphasizes the fact that the kinetics of the crystal growth process is not effected by the details of the underlying microscopic dynamics. We point out that for growth rates larger than 0.2 (in reduced units), further tuning of the thermostating parameters was necessary to melt successfully the crystal at such high velocities. However, the profiles and data presented here were evaluated under more gentle growth conditions (i.e., rates less than 0.1).

Interfacial widths were measured using the same procedure as in our previous work.[8,10] Specifically, the properties of interest were binned and collected in the moving frame along the z direction. For our purposes, we have fixed the moving frame to be the position of the temperature pulse. This assumes that the temperature pulse must follow (at least in an average way) the advancement of the growing interface under steady-state conditions. Since the velocity of the moving frame is no longer constant, but rather determined with some arbitrariness, it follows that the collected data may contain (in addition to capturing the inherent short-time behavior across the interface) some additional information reflecting the fluctuations exhibited by a solid/liquid interface on moderate time scales. Therefore, for some values of C, further broadening may be generated in the profiles collected across an interface and the interfacial width can be expected to depend on this coupling constant. We have found that for a reasonable choice of the coupling constant, $C/\Delta t \approx 10^9-10^{11}$, there is no difference in the measured interfacial width within our error bars.

In Fig. 6, the z profiles of the density, the potential en-

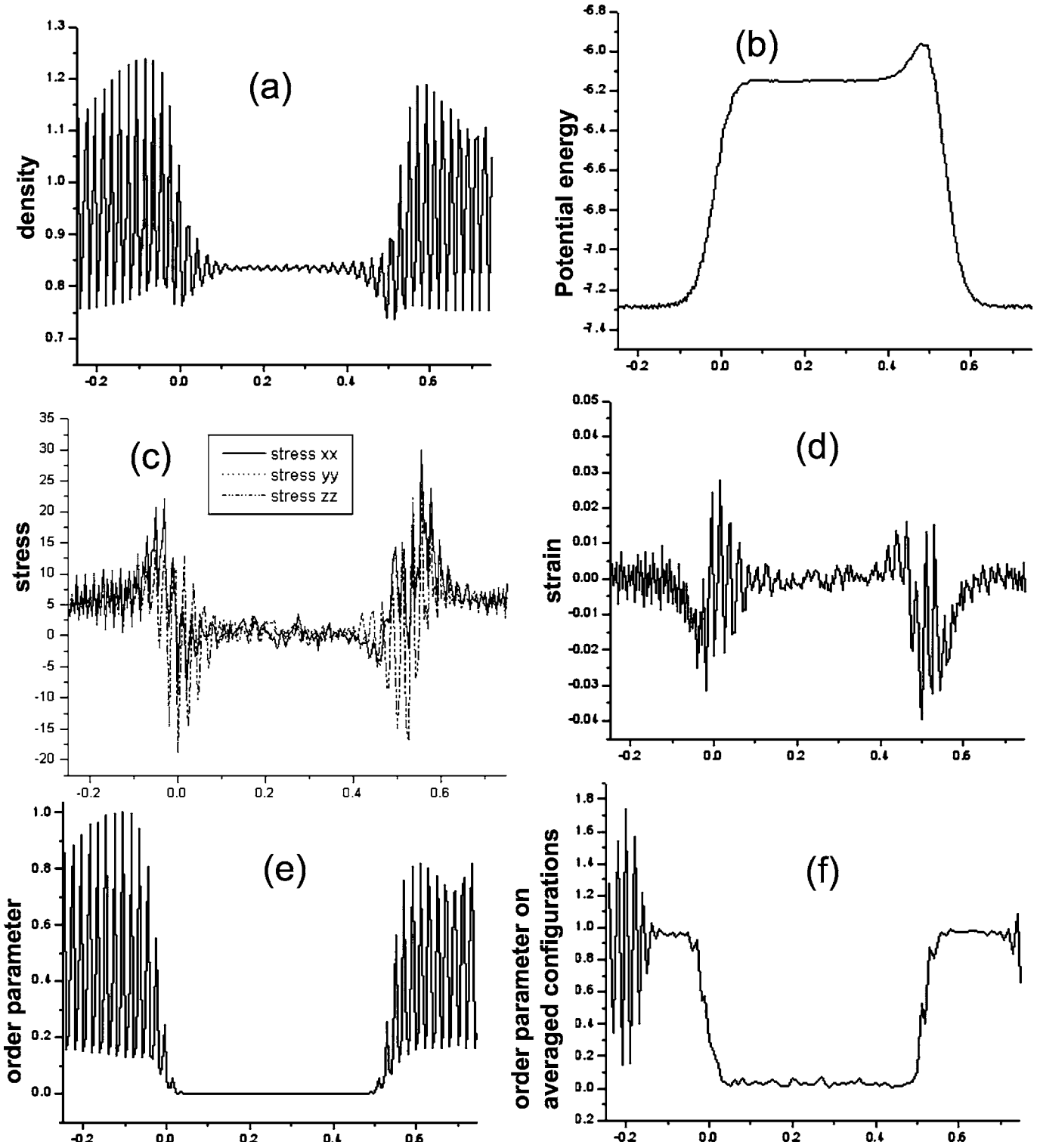

FIG. 6. The z profiles of the (a) density, (b) potential energy, (c) stress, (d) strain=normal stress−tangential stress, (e) $\chi(z)$ order parameter from instantaneous configurations, and (f) $\chi(z)$ order parameter from configurations averaged over 10 000 time steps. The results are for a LJ system growing on the [001] face and represent crude MD data (no smoothing) collected and averaged over 6×10^5 time steps. All results are in reduced units. The x axis on all graphs is the z position along the box (in L_z units) relative to the position of the temperature pulse.

ergy, the xx, yy, and zz components of the pressure, the strain, the order parameter $\chi(z)$ (see Ref. 14) as evaluated from instantaneous configurations, and order parameter $\chi(z)$ as evaluated from time-averaged (over 10 000 time steps) configurations are presented. To provide a direct test of the quality and performance of the present approach, all profiles presented in Fig. 6 are raw MD data without smoothing, sampled and averaged over 600 000 time steps. The density, potential energy, pressure, and strain were binned on a grid of 0.2σ, while the order parameters were binned over 0.4σ. Interestingly, the potential energy profiles are by far the smoothest, while the other profiles require further filtering; this observation is consistent with previous work.[8,10]

An important observation should be made regarding the

quality of the stress profiles. As one can see from Fig. 6(c), the stress profile is smooth enough to determine if it is possible to extract the surface tension γ from the Kirkwood-Buff[20] stress route,

$$\gamma = \frac{1}{2}\sum_{iz}\left\langle \left(p_{zz} - \frac{1}{2}(p_{xx}+p_{yy})\right)_{iz} L_{iz}\right\rangle, \tag{12}$$

where iz is the bin index in the z direction, L_{iz} is the bin width, and p_{xx}, p_{yy}, and p_{zz} are the xx, yy, and zz stress components, respectively. In this context, the strain was defined as the contribution to the surface tension from an individual bin:

$$\text{strain}(z) = \frac{1}{2}\left\langle \left(p_{zz} - \frac{1}{2}(p_{xx}+p_{yy})\right)_{iz} L_{iz}\right\rangle. \tag{13}$$

One can see from Fig. 6(d) that the measured strain in the bulk phases is zero, and therefore its signal over the interface is an integrable quantity that should sum up to the surface tension. However, in all our runs, we have obtained a negative strain signal across our (nonequilibrium) liquid/crystal interfaces that corresponds to a negative surface tension of about −0.1 to −0.18 (in reduced units). The same result was obtained for systems as large as $18\sigma \times 18\sigma$ cross-sectional area, implying that the negative surface tensions were not an artifact of system sizes or simulation conditions. As we do not expect the surface tension of a crystal/liquid interface to be negative, the results suggest that the Kirkwood-Buff route[20] to the surface tension is not applicable to MD simulations of the crystal/liquid interface.

All the collected profiles can be further filtered (smoothed) to remove their high frequency oscillations by the means of Fourier transform filtering to such an extent that numerical derivatives can be calculated. Such smoothed profiles and their numerical derivatives are presented in Fig. 7 for the density, potential energy, and order parameters for a LJ system undergoing steady-state crystal growth. It is evident from Fig. 7 that several well established[8] results for such interfaces are recovered. The position of the interface (identified by the minimum or maximum in the first derivatives of z profiles) and the width of the interface depend somewhat on the measured quantity. The potential energy tends to predict a broader interface than the density or structural order parameters. The widths, quantified by fitting a Gaussian to the extrema in the first derivative, are consistent with results previously reported in the literature,[8,21] although the widths obtained in the present study are typically 0.4–0.6 particle diameters larger than the values reported in Ref. 8. This result is not unexpected; in contrast to the methodology of Ref. 8, the absence of temperature gradients in the present approach allows the interface full freedom to fluctuate around an average position. Further apparent interfacial broadening may result from the present method of measurement. Since the estimated instantaneous rates are no longer constant, imprecision could result from the determination of the position of the interface (i.e., the moving frame) and could therefore lead to further apparent broadening of the

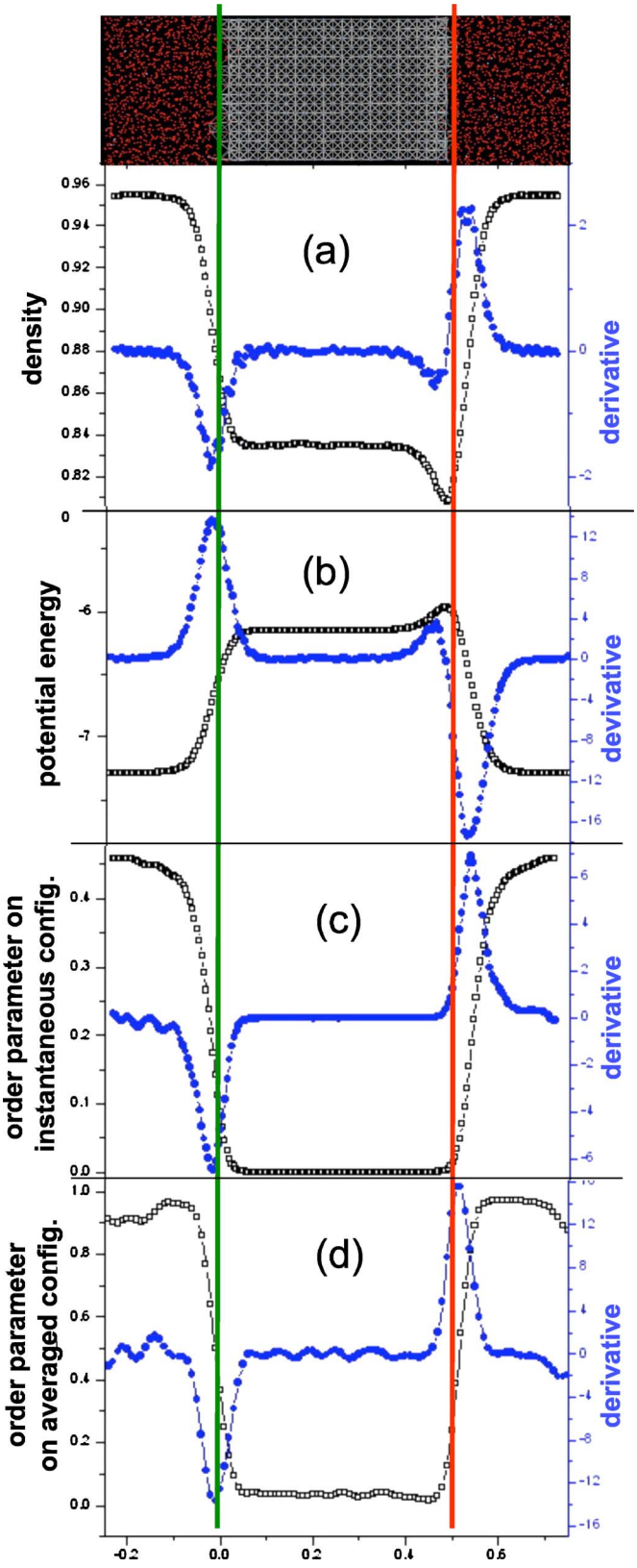

FIG. 7. (Color online) Smoothed profiles for a LJ system while growing on the [001] face. The smoothing was done with special care as not to broaden artificially the sharp increase/decrease at the interfaces. The profiles (black) obtained were then smooth enough to extract first derivatives (blue) and interfacial widths. The units are the same as in Fig. 6. The green and red vertical lines are plotted to help identify the positions of the interfaces.

TABLE III. The measured widths for the liquid/crystal interfaces of the [001], [011], and [111] crystallographic faces of a LJ system. $\chi^{(\text{instant})}$ and $\chi^{(\text{averaged})}$ represent the order parameter $\chi(z)$ evaluated on instantaneous and time-averaged configurations, respectively.

	Face		
Properties	001	011	111
Density	6.2–6.8	5.2–5.6	5–5.4
Potential energy	7.6–8.2	6.2–7.6	6.0–7.4
$\chi^{(\text{instant})}$	5.7–6.4	5.2–5.0	5.2–5.8
$\chi^{(\text{averaged})}$	5.7–6.4	5.2–6.0	5.2–5.8

interface. Hence, considerable care has been taken in this work to provide a robust yet sensitive measure for the position of the interface.

In Table III, values for the interfacial widths as evaluated from density, potential energy, and structural order parameter profiles are presented. We observe that the width of the interface depends somewhat on the crystallographic face. It is apparent from Table III that the interfacial width decreases in the order [001]>[011]>[111]. Both our growth rates and interfacial widths are consistent with results previously reported in the literature.[8,21–23]

Another important question of practical interest is what is the minimum required system size to reliably simulate heterogeneous crystal growth by MD. We have implicitly addressed this question by having performed quite extensive studies of both atomic and molecular systems of different sizes (as described in Sec. III A). From our experience, the two solid/liquid interfaces (in a periodic system) need to be at least 8σ apart in order not to influence each other. Otherwise one of the "bulk" phases is destabilized and the system will either grow or melt too fast. This implies that the length of the simulation box along the direction of asymmetry should be at least 18σ–24σ. In the present work, we have chosen box lengths between 26σ and 41.5σ. The minimum cross-sectional area required to avoid large finite-size effects is $5\sigma\times5\sigma$. However, to capture reliably the fine details of the interfacial structure and kinetics (e.g., interface microfaceting during the growth), interfacial areas of $9\sigma\times9\sigma$ are required. Inspecting the structure of the liquid/crystal interface in a layer by layer fashion as described in Ref. 8, we have noticed that for systems with cross-sectional areas smaller than $9\sigma\times9\sigma$, the crystal growth tends to take place mainly in a layer by layer fashion, with no significant internal structure of the interface being observed. Using larger cross sections (more than the $9\sigma\times9\sigma$ threshold), the interface for any of the crystallographic faces examined appears to readily form islands of crystalline order extending from the solid phase into the liquid phase, similar to that discussed in Ref. 9, and a more complex character of the interface is revealed.

D. Hexagonal ice

We have also tested the present approach on the heterogeneous crystal growth of hexagonal ice I (Fig. 8). For the purposes of the present paper, we emphasize that this framework was successful in growing ice from supercooled water

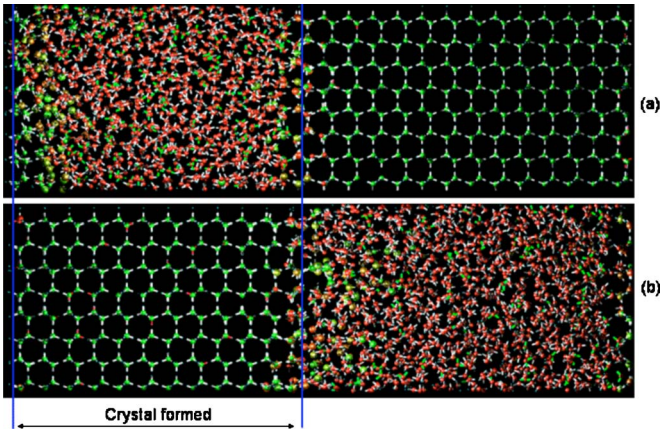

FIG. 8. (Color online) The heterogeneous crystal growth for the [1010] face of hexagonal ice at 265 K. Averaged configurations (a) at $t=0$ and (b) after 11 ns are presented as averaged configurations. The green spheres are water molecules identified as solidlike, while the red spheres are water molecules identified as liquidlike according to the criterion δ_k presented in Sec. III B.

under steady-state conditions. From our simulations, we have found rates of growth of 1.5 Å/ns for 255 K and 4.5 Å/ns for 265 K, in good agreement with results reported in the literature.[24] Interfacial widths for hexagonal ice were about 11–12 Å, as expected.[25] In contrast with LJ systems, we observed for water/ice systems that if a constant growing rate close to its average steady-state value is provided, the system can evolve under an apparent steady state for 10–20 ns (and hence forming 50–60 Å of crystal) before diverging. This is due to the considerably slower growth rates of ice; that is, the fluctuations in the water/ice interface (reflecting competing ordering and disordering processes) are taking place on much larger time scales than for LJ systems. However, longer runs of one-component systems always require a self-adaptive scheme to achieve true steady-state heterogeneous crystal growth.

In Fig. 8 images of the initial (after establishing steady-state) and final averaged configurations from the growth of the [1010] face of ice are presented. From this figure one can see that about 50 Å of new crystal has been formed, while the liquid/crystal ratio has remained almost constant. Clearly, steady-state crystal growth can be maintained and monitored with the present approach.

E. Methane hydrates

In the case of multicomponent crystal growth, there is another factor that can provide feedback to a system trying to reach a steady state, specifically the composition. For example, in the case of methane hydrate crystals, the rate of growth will depend on the level of supersaturation of methane in the aqueous solution at fixed temperature. The growth rate of this two-component crystal will adjust itself according to the thermodynamic driving force, and therefore a steady state can be reached at any rate below a critical threshold (the maximum growth rate). We have found that moderate amounts of methane hydrate sI crystals can be grown at fixed rates below 0.75 Å/ns without requiring a self-adaptive scheme.

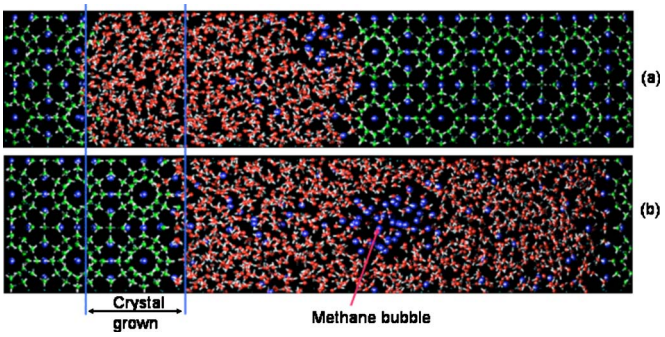

FIG. 9. (Color online) The heterogeneous crystal growth for methane hydrate crystals from solution at 245 K: (a) initial configuration and (b) final configuration after 18 ns. As in Fig. 8, averaged configurations are shown where the molecular color indicates their solidlike or liquidlike character. The methane molecules are represented by blue spheres. Several layers of methane hydrate grew at essentially steady-state conditions over about 9 ns before a methane bubble formed, preventing further crystal growth.

Successful heterogeneous steady-state growth of gas hydrates has in the past proven to be rather challenging because of the mass transport issues associated with the methane in solution and the tendency of methane to demix from a supersaturated aqueous solution.[10,26] To overcome these issues, we have used our technique of active transport, as discussed in Sec. II. Specifically, a small and systematic force was applied to methane molecules to shuttle them away from the melting interface.

In Fig. 9, images of initial and final (after an 18 ns MD trajectory) averaged configurations are presented. About 24 Å of methane hydrate was formed. The final snapshot also shows a bubble of methane that has formed in the system, emphasizing the practical difficulties encountered when simulating the growth of hydrate crystals from methane and water. Before the methane began to demix, the crystal grew at apparently steady-state conditions for about 9 ns.

IV. CONCLUSIONS

In this paper a new MD methodology to simulate the steady-state heterogeneous growth of crystals from their supercooled liquid phases is presented. The systems consist of two interfaces, where at one of them the new crystal is formed while at the other melting occurs. Steady-state growth can be achieved by keeping a constant ratio between the amount of liquid and crystal within the system, that is, by maintaining essentially equal (average) rates for melting and crystallization during the simulation.

In the present simulation methodology, the temperature is controlled on each molecule by a Nose-Hoover chain thermostat. Such an approach affords perhaps the most straightforward method to generate a desired thermal regime in the system for achieving steady-state crystal growth. In this work we utilized a flat temperature profile (with respect to the z direction) with a Gaussian-shaped temperature pulse. The peak of the Gaussian is positioned to coincide with the melting interface, and its role is to provide the heat necessary to melt that interface. Since the temperature is constant over the remainder of the system, heterogeneous crystal growth can be investigated at any desired extent of supercooling. Such an approach provides some advantages over the recently developed method that utilizes two local thermostats and a temperature gradient in the system[8,10] to control its steady state. For example, the absence of a temperature gradient across interface eliminates the artifacts generated by it in various z-profile functions. It also allows the interface to grow under constant and unconstrained conditions, thereby providing more detailed insights into some of the more subtle behaviors (e.g., microfaceting) that contribute to the mechanisms of heterogeneous crystal growth.

One of the crucial issues within the current approach is the control of the system. We have shown that in the absence of a temperature gradient in the system, the system always tends to diverge from its steady state. This behavior is consistent with the large scale (typically over nanoseconds) fluctuations inherent to a growing (melting) interface. A self-adaptive scheme to establish and maintain a desired steady state for the system was developed and tested. Such a scheme monitors the instantaneous rate of growth and moves the temperature pulse (i.e., melting interface) such that the composition of the system is maintained. Two rates are then recorded, the estimated instantaneous and average rates of growth. The latter quantity if of most interest since it should converge to the actual macroscopic rate of growth. The success of the present self-adaptive method of steady-state crystal growth depends critically on a criterion that pinpoints the position of the interface, thereby providing an accurate moving frame from within which to monitor average properties across the interface. A criterion that was able to identify the position of the interface based on even a single instantaneous configuration has been proposed. This criterion exploits the underlining order in the crystal face as manifest in Fourier spectra of either density or structural order parameter profiles. The large fluctuations exhibited by a growing (melting) interface, particularly for molecular systems such as water/ice, necessitate that a well defined moving frame be established to allow the average behavior to be reasonably characterized.

We have demonstrated that the rates of growth and interfacial properties (such as the interfacial width) are well reproduced by this approach. The methodology worked well for both atomic and molecular systems. For example, we were able to achieve steady-state crystal growth of three principal faces of hexagonal ice. In the case of mixtures, there is a reduced need for a self-adaptive scheme; for noncongruent-melting systems the growth rate will be fixed by the thermodynamic force provided by the supersaturation level of components in solution. We have shown that the present approach can be successfully employed to grow the rather demanding methane hydrate system.

Finally, it is important to emphasize again the importance of demonstrating steady-state crystal growth in simulation studies. The work of Tepper and Briels,[27] which showed that interfacial relaxation may be confused with crystal growth behavior in simulations of insufficient duration, provides key support to this argument. While several simulation studies have appeared recently in the literature reporting crystal growth, for example, of ice[24,28,29] or methane hydrates,[30] none of these have achieved steady states

(although all have observed large fluctuations at the interface consistent with the behavior discussed here or in Ref. 27). In the absence of steady-state growth, the interpretation of at least some of such simulation results could thus be problematic. The methodology presented here is very well suited for the investigation of steady-state crystal growth, is reasonably straightforward to implement, and provides an excellent means for examining the average behavior characterizing the solid/liquid interface.

ACKNOWLEDGMENTS

The authors are grateful for the financial support of the Natural Sciences and Engineering Research Council of Canada. The authors also acknowledge M. S. Gulam Razul for useful discussions and WestGrid for providing computational resources.

[1] T. Inabe and H. Tajima, Chem. Rev. (Washington, D.C.) **104**, 5503 (2004); Y. Yeh and R. E. Feeney, *ibid.* **96**, 601 (1996); R. P. Shibaeva and E. B. Yagubskii, *ibid.* **104**, 5347 (2004); P. G. Vekilov and J. I. D. Alexander, *ibid.* **100**, 2061 (2000); S. M. Gates, *ibid.* **96**, 1519 (1996); P. M. Ajayan, *ibid.* **99**, 1787 (1999); N. H. Tran and R. N. Lamb, J. Phys. Chem. B **106**, 352 (2002), and references therein.
[2] K. Haug, M. Lin, and N. J. Lonergan, J. Phys. Chem. B **109**, 14557 (2005); P. A. Thiel and J. W. Evans, *ibid.* **104**, 1663 (2000); M. Mucha and P. Jungwirth, *ibid.* **107**, 8271 (2003); J. Anwar and P. K. Boateng, J. Am. Chem. Soc. **120**, 9600 (1998); D. K. Kondepudi and K. E. Crook, Cryst. Growth Des. **5**, 2173 (2005); T. Li, K. Park, and K. R. Morris, *ibid.* **2**, 177 (2002); P. Bennema, H. Meekes, S. X. M. Boerrigter, H. M. Cuppen, M. A. Deij, J. van Eupen, P. Verwer, and E. Vlieg, *ibid.* **4**, 905 (2004), and references therein.
[3] M. Asta, F. Spaepen, and Fristo van der Veen, MRS Bull. **29**, 920 (2004).
[4] B. Mutaftschiev, *The Atomistic Nature of Crystal Growth* (Springer, Berlin, 2001); R. Davey and J. Garside, *From Molecules to Crystallizers: An Introduction to Crystallization* (Oxford University Press, Oxford, 2000).
[5] J. Q. Broughton and G. H. Gilmer, J. Chem. Phys. **79**, 5095 (1983).
[6] J. Q. Broughton, G. H. Gilmer, and K. A. Jackson, Phys. Rev. Lett. **49**, 1496 (1982).
[7] E. Burke, J. Q. Broughton, and G. H. Gilmer, J. Chem. Phys. **89**, 1030 (1988).
[8] M. S. G. Razul, E. V. Tam, M. E. Lam, and P. G. Kusalik, Mol. Phys. **103**, 1929 (2005).
[9] M. S. G. Razul, J. G. Hendry, and P. G. Kusalik, J. Chem. Phys. **123**, 204722 (2005).
[10] J. Vatamanu and P. G. Kusalik, J. Phys. Chem. B **110**, 15896 (2006).
[11] D. Cyr and P. G. Kusalik (unpublished).
[12] J. Vatamanu and P. G. Kusalik, J. Am. Chem. Soc. **128**, 15588 (2006); Phys. Rev. Lett. (submitted).
[13] S. Nose, J. Chem. Phys. **81**, 511 (1984); W. G. Hoover, Phys. Rev. A **31**, 1695 (1985); G. J. Martyna, M. L. Klein, and M. Tuckerman, J. Chem. Phys. **97**, 2635 (1992).
[14] M. P. Allen and D. J. Tildesley, *Computer Simulation of Liquids* (Clarendon, Oxford, 1989).
[15] H. Nada and J. P. J. M. van der Eerden, J. Chem. Phys. **118**, 7401 (2003).
[16] J. L. Atwood, J. E. D. Davies, and D. D. MacNicol, *Inclusion Compounds: Structural Aspects of Inclusion Compounds Formed by Inorganic and Organic Host Lattices* (Oxford University Press, Oxford, 1991), Vol. 1; T. C. W. Mak and R. McMullan, J. Chem. Phys. **42**, 2732 (1964); R. A. McMullan and G. A. Jeffrey, J. Chem. Phys. **42**, 2725 (1965).
[17] W. L. Jorgensen, J. Chahdrasekhar, J. D. Madura, R. W. Impery, and M. L. Klein, J. Chem. Phys. **79**, 926 (1983).
[18] W. L. Jorgensen, J. D. Madura, and C. J. Swenson, J. Am. Chem. Soc. **106**, 6638 (1984).
[19] U. Essmann, L. Perera, M. L. Berkowitz, T. Darden, H. Lee, and L. G. Pedersen, J. Chem. Phys. **103**, 8577 (1995).
[20] J. G. Kirkwood and F. P. Buff, J. Chem. Phys. **17**, 338 (1949); F. P. Buff and J. G. Kirkwood, *ibid.* **18**, 991 (1950).
[21] A. Kyrlidis and R. A. Brown, Phys. Rev. E **51**, 5832 (1995); R. L. Davidchack and B. B. Laird, *ibid.* **54**, 5905 (1996); B. B. Laird and A. D. J. Haymet, Mol. Phys. **75**, 71 (1992); S. Toxvaerd and E. Praestgaard, J. Chem. Phys. **67**, 5291 (1977); A. J. C. Ladd and L. V. Woodcock, Chem. Phys. Lett. **51**, 155 (1977); Y. Hiwatari, E. Stoll, and T. J. Schneider, J. Chem. Phys. **68**, 3401 (1978); J. Q. Broughton and G. H. Gilmer, *ibid.* **84**, 5749 (1986); **84**, 5759 (1986).
[22] E. Burke, J. Q. Broughton, and G. H. Gilmer, J. Chem. Phys. **89**, 1030 (1988).
[23] J. Q. Broughton and G. H. Gilmer, J. Chem. Phys. **84**, 5759 (1986).
[24] M. A. Carignano, P. B. Shepson, and I. Szleifer, Mol. Phys. **103**, 2957 (2005); H. Nada and Y. Fulurawa, J. Cryst. Growth **283**, 242 (2005).
[25] D. Beaglehole and P. Wilson, J. Chem. Phys. **97**, 11053 (1993); J. A. Hayward and A. D. J. Haymet, *ibid.* **114**, 3713 (2001); J. A. Hayward and A. D. J. Haymet, Phys. Chem. Chem. Phys. **116**, 8876 (2002).
[26] P. M. Rodger, Ann. N.Y. Acad. Sci. **912**, 474 (2000).
[27] H. L. Tepper and W. J. Briels, J. Chem. Phys. **115**, 9434 (2001); **116**, 5186 (2002).
[28] B. F. Nicholson, P. Clancy, and S. W. Rick, J. Cryst. Growth **293**, 78 (2006).
[29] L. Vrbka and P. Jungwirth, Phys. Rev. Lett. **95**, 148501 (2005).
[30] H. Nada, J. Phys. Chem. B **110**, 16526 (2006).